The Astrophysical Journal, 801:93 (10pp), 2015 March 10 doi:10.1088/0004-637X/801/2/93

SOLVING THE PUZZLE OF SUBHALO SPINS

Yang Wang[1,2,4], Weipeng Lin[1,3], Frazer R. Pearce[2], Hanni Lux[2,5], Stuart I. Muldrew[6], and Julian Onions[2]
[1] Key Laboratory for Research in Galaxies and Cosmology, Shanghai Astronomical Observatory, Shanghai 200030, People's Republic of China; wangyang@shao.ac.cn, linwp@shao.ac.cn
[2] School of Physics & Astronomy, University of Nottingham, Nottingham, NG7 2RD, UK
[3] School of Astronomy and Space Science, Sun Yat-Sen University, Guangzhou, 510275, China
[4] Graduate School of the Chinese Academy of Science, 19 A, Yuquan Road, Beijing, China
[5] Department of Physics, University of Oxford, Denys Wilkinson Building, Keble Road, Oxford, OX1 3RH, UK
[6] Department of Physics and Astronomy, University of Leicester, University Road, Leicester, LE1 7RH, UK
Received 2014 November 16; accepted 2015 January 13; published 2015 March 10

ABSTRACT

Investigating the spin parameter distribution of subhalos in two high-resolution isolated halo simulations, recent work by Onions et al. suggested that typical subhalo spins are consistently lower than the spin distribution found for field halos. To further examine this puzzle, we have analyzed simulations of a cosmological volume with sufficient resolution to resolve a significant subhalo population. We confirm the result of Onions et al. and show that the typical spin of a subhalo decreases with decreasing mass and increasing proximity to the host halo center. We interpret this as the growing influence of tidal stripping in removing the outer layers, and hence the higher angular momentum particles, of the subhalos as they move within the host potential. Investigating the redshift dependence of this effect, we find that the typical subhalo spin is smaller with decreasing redshift. This indicates a temporal evolution, as expected in the tidal stripping scenario.

Key words: cosmology: theory – dark matter – galaxies: evolution – galaxies: halos – methods: numerical

1. INTRODUCTION

In the standard model of structure formation, the rotation velocities of disc galaxies are correlated with the spin properties of their surrounding dark matter halos (Fall & Efstathiou 1980). The simplest model explains this correlation via angular momentum conservation and by assuming baryons and dark matter initially share the same specific angular momentum distribution (Mestel 1963). Even though subsequent models paint a more complex picture, this link continues to exist (e.g., Dalcanton et al. 1997; Mo et al. 1998; Navarro & Steinmetz 2000; Abadi et al. 2003; Bett et al. 2010). Consequently, the halo spin is an important parameter in many semi-analytic models of galaxy formation (Kauffmann et al. 1993, 1997; Frenk et al. 1997; Cole et al. 2000; Benson et al. 2001; Bower et al. 2006; Croton et al. 2006; Bertone et al. 2007; De Lucia & Blaizot 2007; Font et al. 2008; Benson 2012) and a number of studies have investigated the spin of individual dark matter halos in cosmological simulations (Peebles 1969; Bullock et al. 2001; Hetznecker & Burkert 2006; Bett et al. 2007; Gottlöber & Yepes 2007; Maccio et al. 2007; Knebe & Power 2008; Antonuccio-Delogu et al. 2010; Wang et al. 2011; Lacerna & Padilla 2012; Bryan et al. 2013; Trowland et al. 2013).

Due to a lack of resolution in previous generations of large cosmological simulations, subhalo spins have not been thoroughly investigated, despite their application within current semi-analytic models (Guo et al. 2011). Initial work by Lee & Lemson (2013) analyzed the spins of the two most massive substructures of Local Group-like systems in the Millennium-II simulation (Boylan-Kolchin et al. 2009) and revealed possible consequences for the application of subhalo spins to near-field cosmology.

Onions et al. (2013) investigated the spin distribution of subhalos in two high-resolution simulations of a Milky Way-like halo (the Aquarius simulation Springel et al. 2008 and the GHALO simulation Stadel et al. 2009) analyzed by a variety of subhalo finders. They suggested that subhalo spins are significantly offset to lower values than those seen in typical distribution functions fitted to halos (Bullock et al. 2001; Bett et al. 2007). This result is independent of the subhalo finder used, so it suggests that this is a true physical effect. This could not be investigated further because their resimulation did not contain a large field halo population. Excluding subhalos, Colín et al. (2004) found the spin parameter distribution of isolated dwarf dark matter halos to be perfectly consistent with that of larger halos. This suggests that the consistently lower spin of substructure is not due to the generally smaller mass of subhalos, but is more likely related to tidal stripping of high angular momentum material. On the other hand, this offset could also be due to differences between the Aquarius and GHALO simulations and those used by Bullock to define the field relation. To answer this question we require a single simulation that simultaneously includes both a significant subhalo and field halo population.

In this work we use purpose built simulations, specifically designed to contain both a field and subhalo population, to investigate the difference in spin distribution functions between subhalos and halos. In Section 2, we present these simulations and the corresponding (sub-)halo catalogs. The different theoretical models of dimensionless spin parameters are described in Section 3, and our results are summarized in Section 4. We discuss our work and conclude in Section 5.

2. SIMULATION DATA

As we require our halo and subhalo masses to span a wide dynamic range ($10^8 \lesssim M \lesssim 10^{15}\,M_\odot$), we have run four dark matter-only comoving cosmological boxes containing 512^3 particles, with linear sizes of 8, 20, 50, and 100 h^{-1} Mpc respectively (hereafter BoxA, BoxB, BoxC, and BoxD). The softening lengths are chosen to be 4% of the mean separation between particles. This set of simulations can both sufficiently resolve subhalo spins (at least 300 particles per subhalo; Bett

Table 1
Summary of Simulation Properties, Halo, and Subhalo Counts for the Halo Finder Indicated

Name	Box size (h^{-1} Mpc)	Particle mass (h^{-1} M_{sub})	Force softening (h^{-1} kpc)	$N_{halo,SUBFIND}$ ⩾300	$N_{halo,HBT}$ ⩾300	$N_{halo,AHF}$ ⩾300	$N_{sub,SUBFIND}$ ⩾300	$N_{sub,HBT}$ ⩾300	$N_{sub,AHF}$ ⩾300
BoxLo	8	2.1×10^6	1.25	1136	⋯	⋯	213	⋯	⋯
BoxA_S1	8	2.6×10^5	0.04	6589	6698	6775	1934	2169	1460
BoxA	8	2.6×10^5	0.63	6651	6587	6798	1651	1899	1216
BoxA_S2	8	2.6×10^5	1.25	6585	6476	6529	1388	1618	944
BoxB	20	4.1×10^6	1.56	8923	8785	9139	2111	2494	1302
BoxC	50	6.5×10^7	3.91	12791	12533	12874	2687	3325	1597
BoxD	100	5.2×10^8	7.81	17562	17053	16901	3072	3949	1737
				⩾2400	⩾2400	⩾2400	⩾2400	⩾2400	⩾2400
BoxA[a]				1132	⋯	⋯	215	⋯	⋯

[a] This higher particle number threshold is used to compare with BoxLo over the same halo mass range.

Table 2
Parameters for the Spin Distribution with Different Substructure Finding Codes and Force Resolution

Peebles Spin		halos		Subhalos	
		λ_0	α	λ_0	α
SUBFIND	BoxA_S1	0.0398 ± 0.00019	2.54 ± 0.039	0.0237 ± 0.00032	3.56 ± 0.13
	BoxA	0.0371 ± 0.00021	2.59 ± 0.047	0.0254 ± 0.00049	2.92 ± 0.17
	BoxA_S2	0.0364 ± 0.00026	2.59 ± 0.058	0.0298 ± 0.00036	2.60 ± 0.10
HBT	BoxA_S1	0.0390 ± 0.00024	2.42 ± 0.049	0.0260 ± 0.00029	2.89 ± 0.10
	BoxA	0.0366 ± 0.00019	2.48 ± 0.042	0.0277 ± 0.00027	2.68 ± 0.08
	BoxA_S2	0.0356 ± 0.00021	2.37 ± 0.046	0.0322 ± 0.00033	2.52 ± 0.08
AHF	BoxA_S1	0.0380 ± 0.00024	2.82 ± 0.053	0.0303 ± 0.00044	2.53 ± 0.12
	BoxA	0.0369 ± 0.00026	2.76 ± 0.059	0.0343 ± 0.00045	2.84 ± 0.11
	BoxA_S2	0.0367 ± 0.00023	2.61 ± 0.051	0.0384 ± 0.00074	3.09 ± 0.17
Bullock Spin		halos		Subhalos	
		λ_0'	σ	λ_0'	σ
SUBFIND	BoxA_S1	0.0308 ± 0.00027	0.655 ± 0.007	0.0123 ± 0.00017	0.827 ± 0.009
	BoxA	0.0310 ± 0.00025	0.629 ± 0.007	0.0167 ± 0.00019	0.664 ± 0.009
	BoxA_S2	0.0320 ± 0.00022	0.615 ± 0.006	0.0224 ± 0.00028	0.629 ± 0.010
HBT	BoxA_S1	0.0303 ± 0.00026	0.638 ± 0.007	0.0150 ± 0.00013	0.754 ± 0.007
	BoxA	0.0309 ± 0.00026	0.626 ± 0.007	0.0198 ± 0.00018	0.674 ± 0.008
	BoxA_S2	0.0320 ± 0.00025	0.605 ± 0.007	0.0262 ± 0.00031	0.644 ± 0.010
AHF	BoxA_S1	0.0278 ± 0.00025	0.677 ± 0.008	0.0178 ± 0.00028	0.768 ± 0.013
	BoxA	0.0283 ± 0.00019	0.655 ± 0.006	0.0248 ± 0.00046	0.761 ± 0.016
	BoxA_S2	0.0290 ± 0.00022	0.613 ± 0.006	0.0323 ± 0.00059	0.779 ± 0.015

et al. 2007) and have significant statistics for halos (c.f. Table 1). We also ran two simulations with the same parameters as those used for the BoxA simulation except for the gravitational softening parameter. BoxA_S1 has a smaller softening length, whereas BoxA_S2 has a larger softening length. We also ran a low-resolution simulation containing 256^3 particles and the same linear size, 8 h^{-1} Mpc, as BoxA, that we designate BoxLo. The mass resolution of BoxA (2.6×10^5 h^{-1} $M_\odot$ per particle) is very close to that of the Aquarius-A simulation at level 4 (Springel et al. 2008), which had a particle mass of 2.7×10^5 h^{-1} $M_\odot$ in the high-resolution region. This mass resolution is roughly three times better than the Millennium-II simulation ($m_p = 6.9 \times 10^6$ h^{-1} $M_\odot$) used by Lee & Lemson (2013). The cosmology was chosen to be the same as in the Aquarius simulation, i.e., ΛCDM with $\Omega_M = 0.25$, $\Omega_\Lambda = 0.75$, $\sigma_8 = 0.9$, $n_s = 1$, $h = 0.73$. Initial conditions were generated at $z = 127$ by the code N-GenIC using the Zel'dovich approximation (written by Volker Springel) to linearly evolve positions from an initially glass-like state. This was then evolved to the present day using GADGET-2 (Springel 2005).

All simulations, except BoxLo, were analyzed with the (sub-)halo-finding code SUBFIND (Springel et al. 2001), AHF (Gill et al. 2004; Knollmann & Knebe 2009), and HBT (Han et al. 2012). BoxLo was only analyzed with SUBFIND. A summary of our simulations is given in Table 1 and details of

Table 3
Parameters Recovered by SUBFIND for the Spin Distribution with Different Mass Resolution

Peebles Spin	halos		Subhalos	
	λ_0	α	λ_0	α
BoxA($N_p \geqslant 300$)	0.0371 ± 0.00021	2.59 ± 0.047	0.0254 ± 0.00049	2.92 ± 0.17
BoxA($N_p \geqslant 2400$)	0.0393 ± 0.00062	2.53 ± 0.13	0.0281 ± 0.0011	2.78 ± 0.33
BoxA_S2($N_p \geqslant 2400$)	0.0389 ± 0.00069	2.48 ± 0.14	0.0288 ± 0.0010	2.51 ± 0.29
BoxLo($N_p \geqslant 300$)	0.0392 ± 0.00073	2.38 ± 0.14	0.0293 ± 0.0008	2.12 ± 0.23
Bullock Spin	**halos**		**Subhalos**	
	λ_0'	σ	λ_0'	σ
BoxA($N_p \geqslant 300$)	0.0310 ± 0.00024	0.629 ± 0.007	0.0167 ± 0.00019	0.664 ± 0.009
BoxA($N_p \geqslant 2400$)	0.0324 ± 0.00060	0.626 ± 0.017	0.0183 ± 0.0008	0.738 ± 0.035
BoxA_S2($N_p \geqslant 2400$)	0.0327 ± 0.00056	0.622 ± 0.016	0.0198 ± 0.0009	0.662 ± 0.040
BoxLo($N_p \geqslant 300$)	0.0337 ± 0.00049	0.616 ± 0.012	0.0207 ± 0.0007	0.582 ± 0.028

all the halo finding algorithms we have used and a discussion of their relative merits can be found in Knebe et al. (2013).

3. THEORY

The dimensionless spin parameter indicates how much a collection of particles is supported by the angular momentum against gravitational collapse, assuming gravitational equilibrium, where a negligible spin parameter represents minimal support, while the value for a completely supported system depends on the chosen parametrization. There are two standard parametrizations defined by Peebles (1969) and Bullock et al. (2001), respectively, that we describe in the following two sections.

Hetznecker & Burkert (2006) showed that Bullock's parametrization is less dependent on redshift evolution than Peebles' parametrization. This is due to it being more stable against variations in the position of the structure's outer radius and therefore not as strongly affected by the many minor mergers over a halo's merging history. Therefore, the two descriptions are not readily interchangeable and results need to be compared using the same parameter.

3.1. Peebles Spin Parameter

Peebles (1969) proposed to parameterize the (sub-)halo spin in the following way:

$$\lambda = \frac{J\sqrt{|E|}}{GM^{5/2}}, \tag{1}$$

where J is total angular momentum, E is the energy, and M is the mass of the (sub-)structure. With this choice, a value of $\lambda \simeq 0.4$ represents a purely rotationally supported object (Frenk & White 2012).

Applying this parametrization, Bett et al. (2007) determined the spin distribution of halos in the Millennium Simulation (Springel et al. 2005). The Millennium Simulation has a mass resolution of $m_p = 8.6 \times 10^8\,h^{-1}\,M_\odot$ and therefore contains very few subhalos. The vast majority of the objects in the TREEclean catalog of Bett et al. (2007) are halos rather than subhalos. The probability density function of log λ they found to fit the distribution used the following parametrization:

$$P(\log\lambda) = A\left(\frac{\lambda}{\lambda_0}\right)^3 \exp\left[-\alpha\left(\frac{\lambda}{\lambda_0}\right)^{3/\alpha}\right], \tag{2}$$

where A is given by,

$$A = 3\ln 10\frac{\alpha^{\alpha-1}}{\Gamma(\alpha)}, \tag{3}$$

and $\Gamma(\alpha)$ is the gamma function. They found $\lambda_0 = 0.04326$ and $\alpha = 2.509$ best fit the distribution of halo spins.

3.2. Bullock Spin Parameter

Bullock et al. (2001) proposed a dimensionless spin parameter of the form:

$$\lambda' = \frac{J}{\sqrt{2}MRV}, \tag{4}$$

where J is the angular momentum within a virilized sphere with radius R and mass M, and V is the circular velocity at the virial radius ($V^2 = GM/R$). They also proposed a parametrization of the probability density function based on Barnes & Efstathiou (1987),

$$P(\lambda') = \frac{1}{\lambda'\sqrt{2\pi}\sigma}\exp\left(-\frac{\ln^2(\lambda'/\lambda_0')}{2\sigma^2}\right). \tag{5}$$

They found the best fit for halos is given by $\lambda_0' = 0.035$ and $\sigma = 0.5$.

4. RESULTS

Note that in this section we will show results for the discrete, normalized derivative of the spin distribution function $\Delta N(<\log\lambda)/\Delta\log\lambda/N_{\rm tot}$ and $\Delta N(<\lambda')/\Delta\lambda'/N_{\rm total}$, while the fitted functions are for the continuous probability density function $P(\log\lambda) = dN(<\log\lambda)/d\log\lambda/N_{\rm total}$ and $P(\lambda') = dN(<\lambda')/d\lambda'/N_{\rm total}$, respectively. For Peebles spin, we set the bin width to be $\Delta\log\lambda = (\log\lambda_{\rm max} - \log\lambda_{\rm min})/100$. For Bullock spin, the bin width is $\Delta\lambda' = (\lambda'_{\rm max} - \lambda'_{\rm min})/100$.

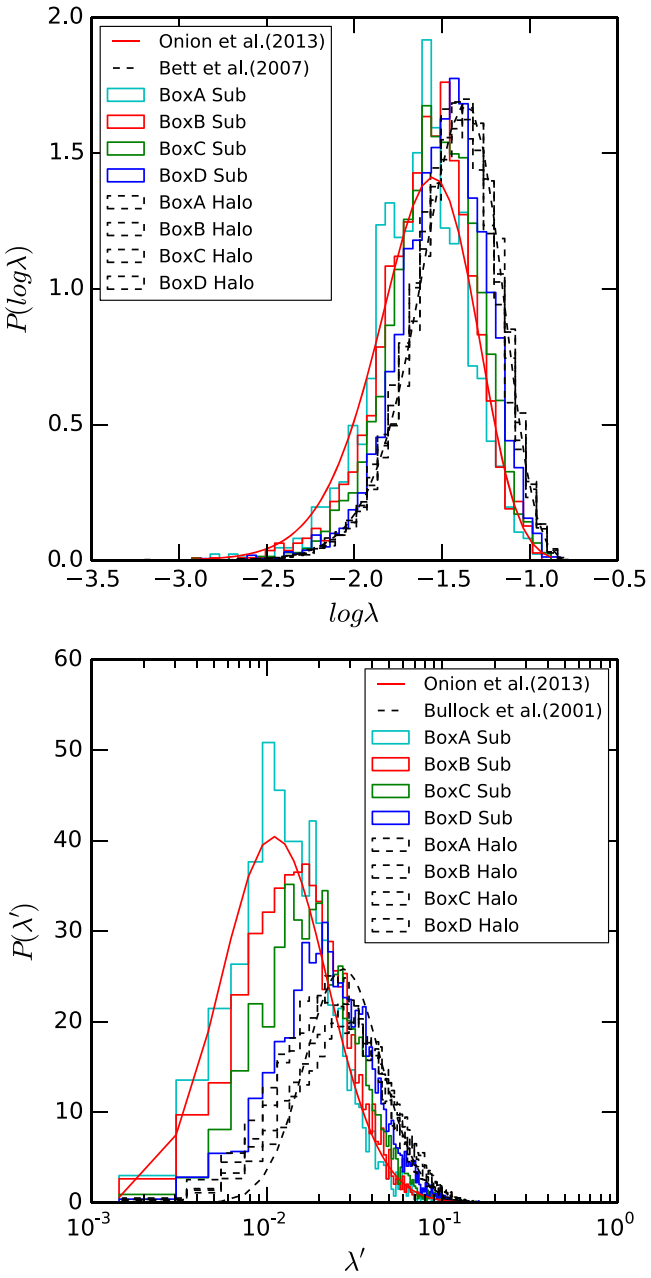

Figure 1. Peebles (upper) and Bullock (lower) spin distribution of SUBFIND (sub-)halos at $z = 0$. The colored solid histograms show the results for subhalos, and the black dashed histogram show it for halos. Two lines show the best fitting functions from Bullock et al. (2001; black dashed line) and Onions et al. (2013; red solid line). Only (sub-)halos with at least 300 particles have been included. For total numbers refer to Table 1.

4.1. Halo Finding Code, Softening, and Resolution Test

In this section, we first test whether the simulation data set and the specific choice of substructure finding code will affect the derived spin of (sub-)halos. Macciò et al. (2008) has tested halo spins with different cosmological parameters. They found that the spin distributions of halos is essentially independent of cosmology, at least for changes between WMAP1, WMAP3, and WMAP5. We choose not to confirm this result here. BoxA, BoxA_S1, and BoxA_S2 are used to compare different force resolutions. BoxA and BoxLo are used to compare different mass resolutions. To ensure reliable properties are recovered, only (sub-)halos with more than 300 particles are selected throughout this work. While calculating the spin of halos, all their substructures are removed. Spin distributions are fitted by Equations (2) and (5), and the fitting parameters are listed in Table 2.

As Table 2 shows, the recovered spin properties of halos are largely independent of the choice of gravitational softening. For subhalos, there is a slight trend for the Peebles spin parameter to increase as the softening is increased, but this effect is only barely resolved. Such a trend would be expected since a larger softening will produce a shallower core potential, lowering slightly the central kinetic energy and altering the energetics and angular momentum profile, thus affecting the spin parameter. For the Peebles measure (Equation (1)), the change in energy is outweighed by the change in angular momentum, but the two effects counteract each other. For the Bullock spin parameter (Equation (4)), only angular momentum has an affect on the spins. So we find that the Bullock spin of subhalos is more sensitive to the softening, as shown in Table 2.

Table 2 also shows that, contrary to Onions et al. (2013), the three halo finding methods do not recover consistent spin parameters. While they all agree on the halo spins, AHF recovers significantly larger spins on average for the subhalo population than either SUBFIND or HBT, which are consistent with each other. The subhalo spins for AHF are broadly consistent with the field population, particularly for larger gravitational softening values. This is also discrepant with Onions et al. (2013), who found lower spin parameter values for their subhalos. This result is due to the failure of AHF to resolve a significant fraction of subhalos within the simulations. The subhalo numbers given in Table 1 indicate that around 36% of the subhalos containing 300 or more particles in BoxA are missed by AHF. The difficulties AHF has resolving substructures where the density contrast between the subhalo and the main halo is expected to be small have also been reported elsewhere (Avila et al. 2014). Further evidence for this issue is the rising incidence of missing substructures as the box size is increased, as evidenced in Table 1: for the largest box (BoxD), AHF missed 25% ∼ 44% of the subhalos found by SUBFIND. AHF is missing small subhalos in the outskirts of the host halo and (as we shall demonstrate later) these small subhalos are precisely the ones with the lowest spin parameters.

This naturally produces a population of subhalos with a higher average spin parameter for AHF. As HBT and SUBFIND produce consistent results, and AHF fails to recover the complete subhalo population, we choose to concentrate our analysis on SUBFIND for the remainder of this paper.

In Table 3 we test the influence of mass resolution. In the brackets after simulation name, we note the particle number threshold chosen. This is set in order to match (sub-)halo masses between BoxA and BoxLo, the lower resolution version of this simulation. This ensures that the halo and subhalo catalogs for BoxLo($N_p \geqslant 300$), BoxA($N_p \geqslant 2400$), and BoxA_S2($N_p \geqslant 2400$) have the same mass range. The gravitational softening lengths for both BoxLo and BoxA were set to 4% of mean particle separation. BoxLo and BoxA_S2 have the same absolute softening length (1.25 h^{-1} kpc). The results show that mass resolution has almost no effect on spin distribution. The first three rows of each sub-table also give a hint about the influence of softening: as suggested above, softening mainly affects the spin of small subhalos. This is not surprising for the reasons already indicated.

Table 4
Parameters for the Spin Distribution Recovered from subfind Halos and Subhalos in Different Mass Ranges

Peebles Spin	halos		Subhalos	
	λ_0	α	λ_0	α
Bett et al. (2007)	0.04326 ± 0.000020	2.509 ± 0.0033[a]	...	...
Onions et al. (2013)	...	...	0.028	3.64
BoxA	0.0371 ± 0.00021	2.59 ± 0.047	0.0254 ± 0.00049	2.92 ± 0.17
BoxB	0.0384 ± 0.00020	2.63 ± 0.043	0.0285 ± 0.00032	2.68 ± 0.09
BoxC	0.0404 ± 0.00018	2.57 ± 0.037	0.0308 ± 0.00033	2.75 ± 0.09
BoxD	0.0411 ± 0.00014	2.47 ± 0.027	0.0346 ± 0.00030	2.54 ± 0.07
Bullock Spin	halos		Subhalos	
	λ_0'	σ	λ_0'	σ
Bullock et al. (2001)	0.035 ± 0.005	0.5 ± 0.3[b]	...	...
Onions et al. (2013)	...	...	0.018[c]	0.70
BoxA	0.0310 ± 0.00024	0.629 ± 0.007	0.0167 ± 0.00019	0.664 ± 0.009
BoxB	0.0332 ± 0.00025	0.632 ± 0.006	0.0199 ± 0.00020	0.669 ± 0.008
BoxC	0.0367 ± 0.00028	0.622 ± 0.006	0.0232 ± 0.00023	0.645 ± 0.008
BoxD	0.0393 ± 0.00027	0.604 ± 0.006	0.0283 ± 0.00025	0.610 ± 0.007

[a] In Bett et al. (2007), the parameters have much smaller uncertainty because there are much lager populations of halos in the work (17,709,121 raw FOF halos including 1,332,239 "clean" ones).
[b] In Bullock et al. (2001), the parameters have larger uncertainty because they use less halos for fitting (only 500 halos).
[c] Note that these parameters differ from the ones originally stated in Onions et al. (2013). The original values were derived using an incorrect fitting routine. The values stated here are the correct values fitted to the Aquarius L4 data set.

4.2. halos versus Subhalos

So far we have seen that the lower spin parameter distribution observed for subhalos appears to be a robust result that does not depend upon the choice of halo finder, gravitational softening, or mass resolution. Here we explore a possible physical origin for the lower subhalo spins.

The left and right panel of Figure 1 show the Peebles spin and Bullock spin distributions of subhalos, as well as halos in all the simulation boxes and the respective fitting functions from Bett et al. (2007), Bullock et al. (2001), and Onions et al. (2013). To assure robustness, only structures resolved with at least 300 particles are included. When we calculate the spin for halos we remove particles contained within substructures. We make fits to the histograms in Figure 1 using Equations (2) and (5). The respective fitting parameters are given in Table 4.

Figure 1 and Tables 2–4 all show that the subhalo spin distribution is different from the halo spin distribution. This further confirms earlier results by Onions et al. (2013), who found that the spin distribution of *subhalos* in the Level 4 resolution Aquarius simulation (Springel et al. 2008) is significantly different than the one derived by Bett et al. (2007) for *halos* in the Millennium Simulation.

Our results reveal new information about the spin of subhalos. As the box size grows from BoxA to BoxD, the discrepancy between λ_0 of halos and subhalos decreases gradually, i.e., the scale of the effect is mass dependent, with larger subhalos tending to have higher spin. One possibility is that in small simulations, such as BoxA or isolated halo models such as Aquarius-A–E studied by Onions et al. (2013), large substructures are generally absent. In the next section we will demonstrate that subhalo spins increase with subhalo mass while halo spins do not have a significant mass dependence.

As an aside, it should be noted that while our fits do not exactly match those given by Bullock et al. (2001), Bett et al. (2007), or Onions et al. (2013), they are within the range of results covered by these works. In practice, previous work does not arrive at an agreement on the exact value of halos' spin. Most of these studies fix λ_0' in the range of 0.031–0.045, with σ between 0.48–0.64 (see Section 4.1 and Figure 7 in Shaw et al. 2006). In Bett et al. (2007), they found median values of $\lambda_{\rm med} = 0.0367 - 0.0429$ for the entire population of halos, depending on the definition of halo, and $\lambda_{med} = 0.043$ for the catalog of halos they refined. Different sets of simulations and halo selection criteria may lead to this variation of the recovered spin parameter. As Section 4.1 demonstrated, such factors as mass resolution and gravitational softening influence the spin. On the other hand, the discrepancy between the spin of halos and subhalos within our simulations is much larger than the bias among simulations. It should therefore be regarded as an intrinsic physical property rather than a result of different data sets.

4.3. Mass Dependence

As we suggest above, mass dependence can explain the discrepancy between the spins of halos and subhalos. To validate this, we further explore the mass dependence of (sub-) halo spin. Figures 2 and 3 show the two-dimensional histogram of spin against (sub-)halo mass. They present a straightforward picture of how the spin distribution changes with mass. We use four simulations to expand the mass range. Contours for each simulation at the same redshift are normalized and stacked together into one subplot. We then divide the sample into 40 bins by log((sub-)halo mass), and fit the distribution by Equations (2) and (5) (if the sample volume in that bin is large enough). $\lambda_0(\lambda_0')$ in each mass bin is calculated and marked on the plots with a cross, and a linear fit to $\lambda_0(\lambda_0')$ against mass is indicated by the red solid line. From the subplots corresponding to redshift 0 (top left and top right), we can see that, for subhalos, $\lambda_0(\lambda_0')$ clearly increases with increasing subhalo mass. In contrast, the spin distribution of halos is almost

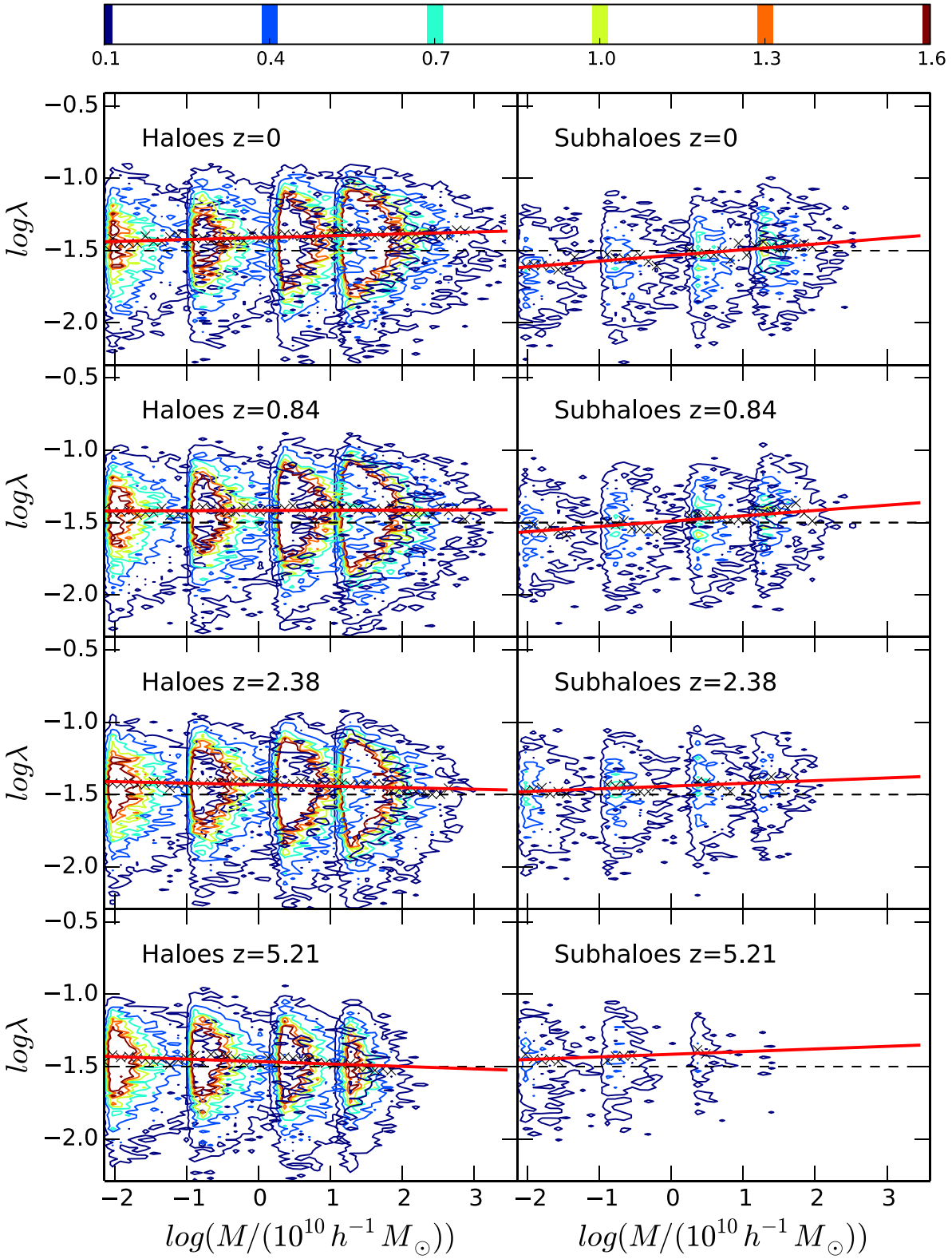

Figure 2. Two-dimensional histogram of Peebles spin against SUBFIND (sub-)halos mass. Contours with different colors represent different levels of number density (calculated as $dN/dlog\lambda/dlog(M/10^{10}\,h^{-1}\,M_{\odot})/10{,}000$), as indicated in the color bar above. Subplots in the left column are statistics for halos and those in the right column are for subhalos. Two plots in the same row are from the same snapshot. The redshift of each row increases from top to bottom, respectively. There are, in fact, four parts of contour in each subplot, which come from our four simulations respectively. The cross scatters represent λ_0 in every mass bin. The thick red lines are linear, fitting to λ_0 against mass. The black dashed line indicates a position of $log\ \lambda = -1.5(\lambda \approx 0.032)$ as a standard for comparison.

independent of mass. The increasing subhalo spin with mass is even more pronounced for the Bullock spin parameter shown in Figure 3 because, for the Bullock spin, the (sub-)halo mass has a higher weight (c.f. Equations (1), (4)). This results in a larger discrepancy between halos and subhalos at the low-mass end. The samples in Onions et al. (2013) are from a Milky-Way-like

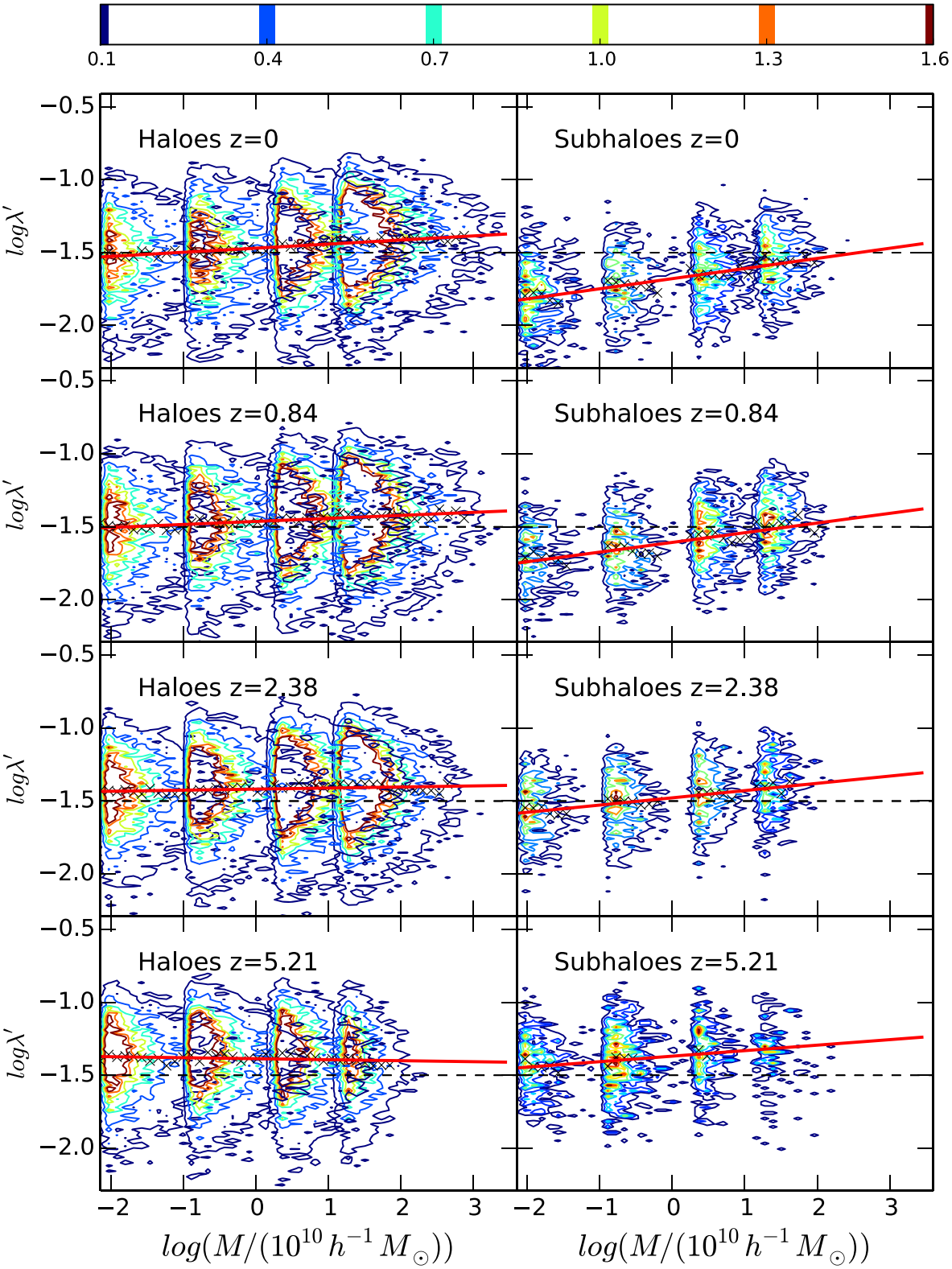

Figure 3. Two-dimensional histogram of Bullock spin against SUBFIND (sub-)halos mass. Contours with different colors represent different levels of number density (calculated as $dN/d\log\lambda'/d\log(M/10^{10}\mathrm{h}^{-1}M_{\odot})/10{,}000$), as indicated in the color bar above. Subplots in left column are statistics for halos and and those in the right column are for subhalos. Two plots in the same row are from the same snapshot. The redshift of each row increases from top to bottom, respectively. There are, in fact, four parts of contour in each subplot, which come from our four simulations respectively. The cross scatters represent λ_0' in every mass bin. The thick red lines are linear fitting to λ_0' against mass. The black dashed line indicates a position of $\log\lambda' = -1.5(\lambda' \approx 0.032)$ as a standard for comparison.

resimulation, which contains subhalos similar to those found in BoxA. So the subhalo spin distribution in their work is closer to that from BoxA. Onions et al. (2013) suggest that the physical mechanism that drives this difference is mass stripping.

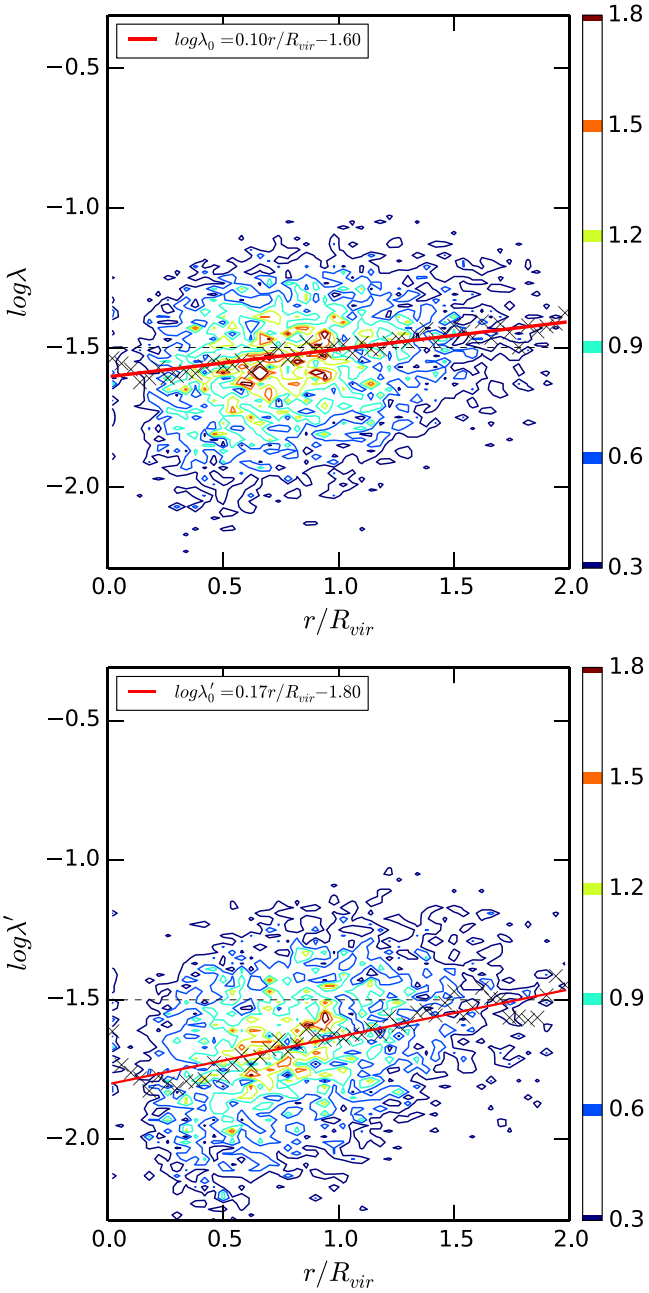

Figure 4. The average Peebles (upper) and Bullock (lower) spin distribution of SUBFIND subhalos against their relative distance from the host halo center. r is the distance of subhalos from the center of their host halo. $R_{\rm vir}$ is the virial radius of the host halo. The crosses indicate the peak of every radial bin and the red line is a linear fitting to these marks. Contours with different colors represent different levels of number density (calculated as $dN/d\log\lambda(or\lambda')/d\log r/R_{\rm vir})/10000$), as indicated in the color bars to the right.

Subhalo particles with high angular momentum are stripped preferentially, which leads to a decrease in the spin parameter. Subhalos with low mass are usually the ones stripped most severely. Our results strongly support the claims Onions et al. (2013) made.

The slightly positive slope of $\lambda_{0,\rm halo}(M_{\rm halo})$ and $\lambda'_{0,halo}(M_{\rm halo})$ is inconsistent with some previous work. They found that $\lambda_{0,\rm halo}$ is constant or has a slightly negative slope (c.f. Bett et al. 2007; Maccio et al. 2007). However we should not forget this trend includes the effect of systematic bias between simulations. Figure 10 in Macciò et al. (2008) shows that $\lambda'_0(M_{\rm halo})$ has a slope of 0.005 in a simulation using WMAP1, which is the same cosmology as used here.

Table 5
Parameters for Fitted Lines for Spin Against (Sub-)Halo Mass

		$\log\lambda_0 = a * \log(M/10^{10}\,{\rm h}^{-1}\,M_\odot) + b$			
	Redshift	Halo		Subhalo	
		a	b	a	b
Peebles spin	0	0.013	−1.41	0.039	−1.53
	0.84	0.0015	−1.42	0.037	−1.49
	2.38	−0.010	−1.43	0.018	−1.44
	5.21	−0.017	−1.46	0.018	−1.41
		$\log\lambda'_0 = a * \log(M/10^{10}\,{\rm h}^{-1}\,M_\odot) + b$			
		Halo		Subhalo	
		a	b	a	b
Bullock spin	0	0.028	−1.47	0.069	−1.68
	0.84	0.021	−1.46	0.066	−1.61
	2.38	0.0073	−1.42	0.047	−1.47
	5.21	−0.0068	−1.39	0.037	−1.37

4.4. Radial Dependence

To understand further whether tidal stripping of high angular momentum material could cause the lower subhalo spin distribution, we investigate the radial dependence of the subhalo spins. Subhalos located closer to the center of their host halo are likely to have undergone stronger tidal stripping than those nearer the virial radius. Onions et al. (2013) has done some tests to support their argument, e.g., they analyze the average spin parameter of subhalos at different distances from the center of the host halo. Here we perform a more detailed test. We stack subhalo samples from four simulations together and then make the two-dimensional histogram of spin against their centric distance. Then, in each radial bin, we fit the subhalo sample using Equations (2) and (5). Finally, we make a linear fit as $\lambda_0(r) = cr/R_{\rm vir} + d$ or $\lambda'_0(r) = cr/R_{\rm vir} + d$. The results are displayed in Figure 4 and show that the spin of subhalos is suppressed close to the center of the host halo. This is consistent with the argument that subhalos lose their high angular momentum particles as they are stripped of their outer layers after infall into a main halo.

4.5. Redshift Dependence

So far, all our analysis was conducted on the $z = 0$ snapshot. However, the spin distribution is known to change with redshift (Hetznecker & Burkert 2006). Hence, we investigated the redshift dependence of the halo versus subhalo spin distribution offset. In Figures 2 and 3, we give the Peebles and Bullock spin distributions of (sub-)halos at $z = 0$, $z = 0.84$, $z = 2.38$, and $z = 5.21$, respectively. The spin of subhalos at the lower mass end decreases significantly with time, while the spin of massive halos increases slightly with time. We calculate the $\lambda_0(\lambda'_0)$ in each mass bin and then use a linear function $\log\lambda_0 = a^* \log(M/10^{10}\,{\rm h}^{-1}\,M_\odot) + b$ (λ'_0 for Bullock spin) to fit $\lambda_0(\lambda'_0)$ against mass. We list the parameters of each fitting line in Table 5. It is clear that the difference between the halo and subhalo spin distribution increases with time. This is

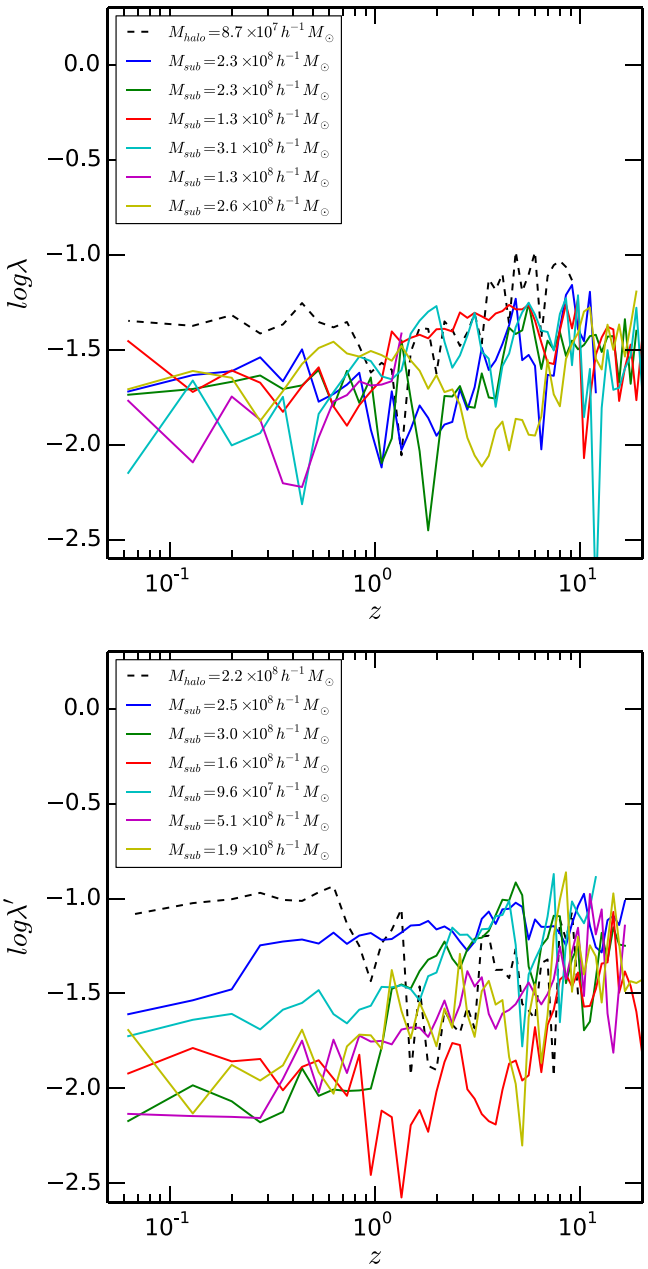

Figure 5. The evolution of Peebles (upper) and Bullock (lower) spin of six selected subhalos from BoxA. Subhalos have at least 300 particles and are less massive than $10^9\,h^{-1}\,M_{\odot}$. All selected subhalos form prior to redshift 8. Solid colored lines represent different subhalos. The black dashed line shows the spin of a halo changing with time as a reference.

consistent with the argument that tidal stripping causes the difference. Affected by stripping, subhalos loose more and more high angular momentum particles as time passes.

To confirm this result we checked how the spin of a single halo changes with time. We randomly select six subhalos and plot their spin against redshift. We constrain the samples selected so that they are likely to be the heavily stripped subhalos. As expected, heavily stripped subhalos should have low mass (here we choose masses less than $10^9\,h^{-1}\,M_{\odot}$) and have long histories, forming prior to redshift 8. As shown in Figure 5, the spin of subhalos declines at low redshift. We have checked many more subhalos not displayed in Figure 5 and we find that most of them display the same trend. We also plot a dashed line for a halo as reference. The halo is in the same mass range as the subhalos selected. Its spin almost does not change at low redshift. This piece of evidence strongly supports the claim that subhalos suffer from stripping, loosing their spin over time.

The information at the high redshift end in Figure 5 is not reliable since the progenitors do not contain very many particles. This results in the large fluctuations seen here.

5. DISCUSSION AND CONCLUSIONS

In this work we compared the spin distribution function of halos and subhalos in sets of cosmological box simulations. We found that the *halo* spin distribution function is well fitted by the parametrizations given by Bullock et al. (2001) and Bett et al. (2007) for the Bullock and Peebles (Peebles 1969) spin parameter, respectively. For the *subhalo* spin distribution function, however, the typical spin of a small subhalo is significantly lower. This was previously suggested by Onions et al. (2013) for the subhalos within Milky Way-like halos, but is confirmed here for a full cosmological volume.

We investigated the origin of the difference between the halo and subhalo spin distributions. We examined the influence of (sub-)halo finder, spin parametrization, and resolution to confirm that these factors are not the origin of the difference between the halo and subhalo spin distributions. In this process we confirmed the difficulties that the AHF finder has in recovering substructures reliably where the density contrast between the main halo and the subhalo is low. We recommend that the AHF halo finder should be treated with caution in situations where a complete unbiased sample of the subhalo population is required.

In this paper, we have argued that the difference between the spin distributions is physical and is caused by tidal stripping of subhalos removing high angular momentum material. This argument is strongly supported by three pieces of evidence presented here. First, subhalos tend to have lower spin when compared to halos of the same mass. This discrepancy gets larger toward the low-mass end. Second, the spin distribution of subhalos is radially dependent within a host halo. Subhalos closer to the host halo center, which are expected to have been more tidally stripped, have lower spin than those closer to the virial radius. Third, the difference between halo and subhalo spin increases with time and, hence, is being caused by a dynamical effect, such as tidal stripping.

In summary, we have demonstrated that subhalos typically have lower spin than halos because tidal stripping removes their highest angular momentum material. This can have an important consequence for galaxy properties that require spin parameter information. Galaxy properties that are related to spin are more likely to be correlated to the spin of the subhalo before infall and not necessarily to its present value.

This work was supported by the NSFC projects (grant Nos. 11473053, 11121062, 11233005, U1331201), the National Key Basic Research Program of China (grant No. 2015CB857001), and the "Strategic Priority Research Program the Emergence of Cosmological Structures" of the Chinese Academy of Sciences (grant No. XDB09010000). Y.W. was supported by the EC framework 7 research exchange program LACEGAL. H.L. acknowledges a fellowship from the European Commissions Framework Programme 7, through the Marie Curie Initial Training Network CosmoComp (PITN-GA-2009–238356). S.I.

M. acknowledges the support of the STFC Studentship Enhancement Programme (STEP) and the support of a STFC consolidated grant (ST/K001000/1) to the astrophysics group at the University of Leicester. Part of the simulations in this paper were performed on the High Performance Computing (HPC) facilities at the University of Nottingham (www.nottingham.ac.uk/hpc). This work also made use of the High Performance Computing Resource in the Core Facility for Advanced Research Computing at Shanghai Astronomical Observatory.

The authors contributed to this paper in the following way: Y. W. led the project and is a PhD student of W.P.L., currently undertaking an extended exchange with F.R.P.; Y.W. conducted the simulation and analysis with assistance from S.I.M. and J.O.; and the manuscript was prepared by Y.W., H.L., and S.I.M., with comments and contributions from all authors.

Y.W. also acknowledges Jiaxin Han and Zhaozhou Li for their support on HBT.

REFERENCES

Abadi, M. G., Navarro, J. F., Steinmetz, M., & Eke, V. R. 2003, ApJ, 591, 499
Antonuccio-Delogu, V., Dobrotka, A., Becciani, U., et al. 2010, MNRAS, 407, 1338
Avila, S., Knebe, A., Pearce, F. R., et al. 2014, MNRAS, 441, 3488
Barnes, J., & Efstathiou, G. 1987, ApJ, 319, 575
Benson, A. J. 2012, NewA, 17, 175
Benson, A. J., Pearce, F. R., Frenk, C. S., Baugh, C. M., & Jenkins, A. 2001, MNRAS, 320, 261
Bertone, S., de Lucia, G., & Thomas, P. A. 2007, MNRAS, 379, 1143
Bett, P., Eke, V., Frenk, C. S., et al. 2007, MNRAS, 376, 215
Bett, P., Eke, V., Frenk, C. S., Jenkins, A., & Okamoto, T. 2010, MNRAS, 404, 1137
Bower, R. G., Benson, A. J., Malbon, R., et al. 2006, MNRAS, 370, 645
Boylan-Kolchin, M., Springel, V., White, S. D. M., Jenkins, A., & Lemson, G. 2009, MNRAS, 398, 1150
Bryan, S. E., Kay, S. T., Duffy, A. R., et al. 2013, MNRAS, 429, 3316
Bullock, J. S., Dekel, A., Kolatt, T. S., et al. 2001, ApJ, 555, 240
Cole, S., Lacey, C. G., Baugh, C. M., & Frenk, C. S. 2000, MNRAS, 319, 168
Colín, P., Klypin, A., Valenzuela, O., & Gottlöber, S. 2004, ApJ, 612, 50
Croton, D. J., Springel, V., White, S. D. M., et al. 2006, MNRAS, 365, 11
Dalcanton, J. J., Spergel, D. N., & Summers, F. J. 1997, ApJ, 482, 659
De Lucia, G., & Blaizot, J. 2007, MNRAS, 375, 2
Fall, S., & Efstathiou, G. 1980, MNRAS, 193, 189
Font, A. S., Bower, R. G., McCarthy, I. G., et al. 2008, MNRAS, 389, 1619
Frenk, C., & White, S. 2012, AnP, 524, 507
Frenk, C. S., Baugh, C. M., Cole, S., & Lacey, S. 1997, in ASP Conf. Ser. vol. 117, Dark and Visible Matter in Galaxies and Cosmological Implications, ed. M. Persic, & P. Salucci (San Francisco, CA: ASP), 335
Gill, S. P., Knebe, A., & Gibson, B. K. 2004, MNRAS, 351, 399
Gottlöber, S., & Yepes, G. 2007, ApJ, 664, 117
Guo, Q., White, S., Boylan-Kolchin, M., et al. 2011, MNRAS, 413, 101
Han, J., Jing, Y. P., Wang, H., & Wang, W. 2012, MNRAS, 427, 2437
Hetznecker, H., & Burkert, A. 2006, MNRAS, 370, 1905
Kauffmann, G., Nusser, A., & Steinmetz, M. 1997, MNRAS, 286, 795
Kauffmann, G., White, S. D. M., & Guiderdoni, B. 1993, MNRAS, 264 201
Knebe, A., Pearce, F. R., Lux, H., et al. 2013, MNRAS, 435, 1618
Knebe, A., & Power, C. 2008, ApJ, 678, 621
Knollmann, S. R., & Knebe, A. 2009, ApJS, 182, 608
Lacerna, I., & Padilla, N. 2012, MNRAS, 426, L26
Lee, J., & Lemson, G. 2013, JCAP, 5, 22
Macciò, A. V., Dutton, A. A., & van den Bosch, F. C. 2008, MNRAS, 391, 1940
Macciò, A. V., Dutton, A. A., van den Bosch, F. C., et al. 2007, MNRAS, 378, 55
Mestel, L. 1963, MNRAS, 126, 553
Mo, H. J., Mao, S., & White, S. D. M. 1998, MNRAS, 295, 319
Navarro, J. F., & Steinmetz, M. 2000, ApJ, 538, 477
Onions, J., Ascasibar, Y., Behroozi, P., et al. 2013, MNRAS, 429, 2739
Peebles, P. 1969, ApJ, 155, 393
Shaw, L. D., Weller, J., Ostriker, J. P., & Bode, P. 2006, ApJ, 646, 815
Springel, V. 2005, MNRAS, 364, 1105
Springel, V., White, S. D. M., Tormen, G., & Kauffmann, G. 2001, MNRAS, 328, 726
Springel, V., White, S. D. M., Jenkins, A., et al. 2005, Natur, 435, 629
Springel, V., Wang, J., Vogelsberger, M., et al. 2008, MNRAS, 391, 1685
Stadel, J., Potter, D., Moore, B., et al. 2009, MNRAS, 398, L21
Trowland, H. E., Lewis, G. F., & Bland-Hawthorn, J. 2013, ApJ, 762, 72
Wang, H., Mo, H. J., Jing, Y. P., Yang, X., & Wang, Y. 2011, MNRAS, 413, 1973